A Technique for Mapping Thermal Infrared Radiation Variation Within Land Cover

Kazuo Oki and Kenji Omasa

***Abstract*—In this letter, a technique for mapping the thermal infrared radiation variation within land cover using both a classification map and a thermal infrared image is proposed. Furthermore, a technique to effectively calculate the average thermal radiance for each land cover from Thematic Mapper (TM)-type sensors, which aquire high resolution of visible and near-infrared images and low resolution of thermal infrared images, was also proposed. These techniques provide useful information on processing TM-type sensors for urban heat monitoring, vegetation diagnosis monitoring, forest fire monitoring, and so forth.**

***Index Terms*—Mixed pixel, thermal infrared image, urban heat, vegetation diagnosis.**

I. Introduction

THERMAL INFRARED images observed by remote sensing provide useful information in evaluating the environmental conditions of land and water areas. For example, information regarding plankton and El Niño is used in helping fisheries [1], [2] and evaluating influences on the global environment, such as global warming. Information regarding the condition of areas of land is used in evaluating the urban heat effect, vegetation transpiration, volcanic activities, and other phenomena. However, current thermal infrared sensors for satellite remote sensing have low spatial resolutions. As a result, an observed pixel contains multiple categories (mixed pixels).

Some researchers have reported studies regarding the problems of mixed pixels [3]–[7] and low spatial resolutions in infrared thermal imaging [8]–[11]. These studies are based on the assumption that temperatures are equal throughout the same land cover type [8]–[11]. However, this assumption is often not true when the selected area is wide. For example, the urban heat phenomenon may make the ground surface temperature in a metropolitan area different from that in an area categorized as the same urban area. Even the same species of vegetation may show different leaf temperatures, depending on a different transpiration rate [12].

In this letter, the thermal infrared radiance from each land cover in low spatial resolution images using visible and near-infrared (NIR) images of higher spatial resolutions was estimated, and a technique of extracting abnormal thermal infrared radiation areas based on the fact that temperatures are not equal throughout the same category was proposed.

Manuscript received June 12, 2002; revised April 2, 2003.

The authors are with the Graduate School of Agricultural and Life Sciences, The University of Tokyo, Tokyo 113-8657, Japan (e-mail: agrioki@mail.ecc.u-tokyo.ac.jp; aomasa@mail.ecc.u-tokyo.ac.jp).

Digital Object Identifier 10.1109/TGRS.2003.813697

II. Estimating Thermal Infrared Radiance of Each Land Cover

A. Linear Mixture Model

A thermal infrared image with low spatial resolution generally contains multiple categories within a pixel (mixed pixels). Therefore, a thermal infrared image should be analyzed, taking the influence of each category into consideration.

If atmospheric influences can be ignored and temperatures in the same category are equal throughout the thermal infrared image, then the thermal infrared radiance (watts per square meter steradian micron) of a pixel (E) can be expressed as the thermal infrared radiance representing each category (Em) as follows:

$$E = \sum_{j=1}^{k} a_j \cdot E_{mj}. \tag{1}$$

However

$$\sum_{j=1}^{k} a_j = 1 \tag{2}$$

$$a_j \geq 0 \tag{3}$$

where a and k are the coverage of each category within a pixel and the number of categories. If Em in (1) can be estimated, the thermal infrared radiance in each category can be analyzed with higher precision.

B. Determining Thermal Infrared Radiance of Each Category

We used visible and NIR images of Landsat Thematic Mapper (TM) (spatial resolution: 30 m), which has higher spatial resolutions than thermal infrared image of Landsat TM (spatial resolution: 120 m), to determine Em. In this letter, we used digital numbers (DNs) in order to express thermal infrared radiance of thermal infrared images. E and Em are proportional to DNs used in thermal infrared images of Landsat TM, since the TM thermal band is calibrated on a linear relationship between DN and radiance. Fig. 1 shows a false-color image of the Kanto Area in Japan observed on April 19, 1993, and Fig. 2 shows the thermal infrared image.

To determine Em from (1), E (thermal infrared radiance of a pixel) and a (coverage of each category within a pixel) is required. The thermal infrared radiance of a pixel can be obtained from the observed image. To calculate the coverage of each category within a pixel of a thermal infrared image of Landsat TM, land covers with a number of categories were classified using

0196-2892/03$17.00 © 2003 IEEE

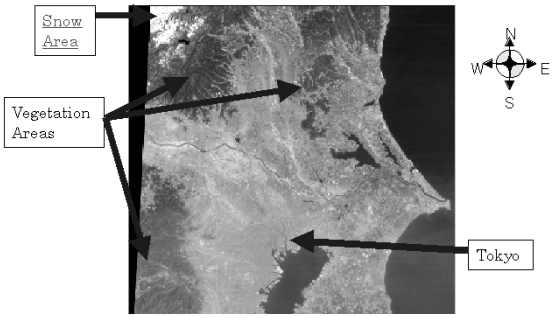

Fig. 1. False-color image of the Kanto Area in Japan observed on April 19, 1993.

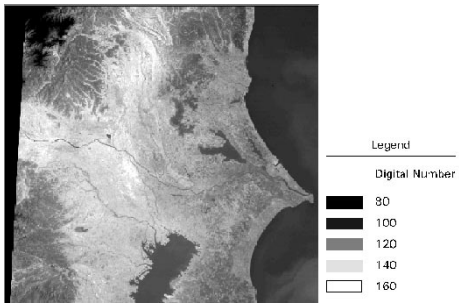

Fig. 2. Thermal infrared image of Landsat TM.

six bands of the visible and NIR images of higher spatial resolutions. Then, the thermal infrared image was overlaid on the classified Landsat image. From the overlaid image, the coverage of each category within a pixel was determined for a Landsat TM thermal infrared image.

From the calculated coverage of each category and the known thermal infrared radiance of a pixel in the thermal infrared image, the unknown thermal infrared radiance in each category was estimated by the least squares method using (1) and under the conditions of (4) [13]

$$E_{mj} \geq 0. \tag{4}$$

Each category in the classified Landsat image must be ideally the same land cover type. However, in general, it is difficult to determine the optimal number of categories within an image, since the user has to subjectively decide the categories or the number for the purpose of research.

There may be a more optimal number of categories, but in this study, the Landsat Image was classified into 15 categories, in order to separate urban and snow area and to consider each land cover type or same land cover type within the image. Here, we assumed that the optimal number of categories is 15. Fig. 3 shows the image classified by the ISODATA method using six bands, the visible and NIR images, of Landsat TM observed on April 19, 1993. Table I lists the estimated thermal infrared radiance for each category. The classified categories roughly consist of water, vegetation, urban area, snow area, and bare soil. Ideally, we want to decide the name of land use or land cover for the 15 categories, but it is difficult to specify what each category is.

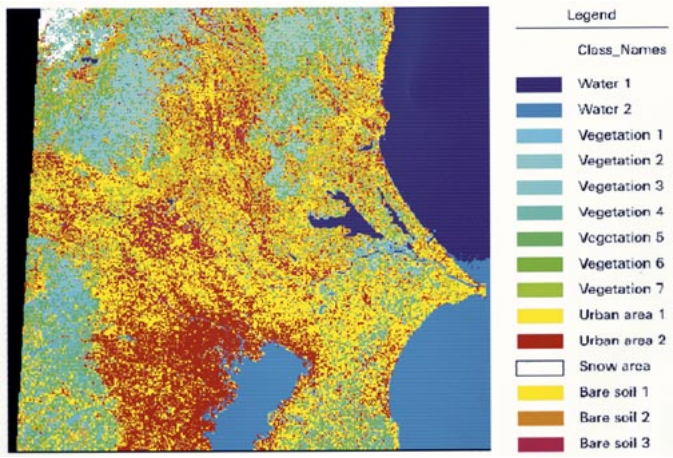

Fig. 3. Image classified by the ISODATA method using six bands of the visible and NIR images of Landsat TM observed on April 19, 1993.

C. Image of Thermal Infrared Radiance From Each Land Cover

By substituting the estimated Em in the classified image in Fig. 3, the resolution of the thermal infrared image shown in Fig. 2 is finer. Fig. 4 shows the estimated fine image of the thermal infrared radiance from each land cover.

The estimated fine image in Fig. 4 is based on the assumptions that atmospheric influences can be ignored throughout the image and that temperatures are equal throughout the same category [3]–[6].

III. Extracting Information on Abnormal Thermal Radiation From Each Land Cover

The estimated fine image shown in Fig. 4 is based on the assumption that the temperature is equal throughout the same category. However, this assumption is often not true, due to factors such as urban heat phenomenon and plant transpiration. Thus, a new technique for extracting an area of abnormal thermal radiation was developed, based on the fact that the temperature is not equal throughout the same category. If several influences produce a temperature difference even in the same category, then the thermal infrared radiation radiance in a pixel of an infrared-band image should not be expressed as in (1) but as follows:

$$E = \sum_{j=1}^{k} a_j \cdot E_{mj} + \Delta E \tag{5}$$

where ΔE is the difference between the observed and estimated thermal infrared energies based on the assumption that the temperatures are equal throughout the same category. In other words, an area with abnormal thermal radiation in each category can be extracted from a thermal infrared image by evaluating ΔE with (6)

$$\Delta E = E - \sum_{j=1}^{k} a_j \cdot E_{mj}. \tag{6}$$

ΔE expresses a positive or negative value. A large positive value indicates high thermal infrared radiance, while a large

TABLE I
ESTIMATED THERMAL INFRARED RADIANCE (DN) FOR EACH CATEGORY

Water 1	Water 2	Vegetation 1	Vegetation 2	Vegetation 3
104.9	106.7	117.7	113.9	117.6
Vegetation 4	Vegetation 5	Vegetation 6	Vegetation 7	Urban area 1
92.1	113.9	119.1	130.4	129.1
Urban area 2	Snow area	Bare soil 1	Bare soil 2	Bare soil 3
133.7	87.6	135.4	131.3	138.6

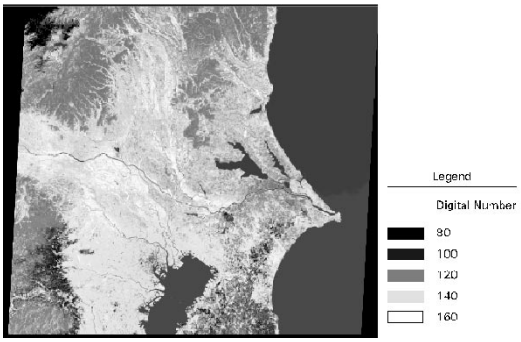

Fig. 4. Estimated fine image of the thermal infrared radiance from each land cover.

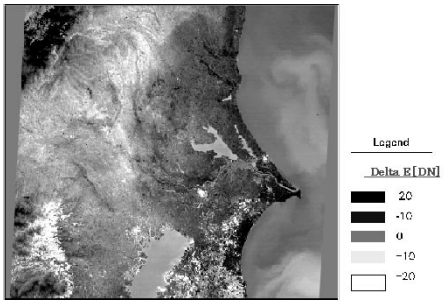

Fig. 5. ΔE image calculated from (6).

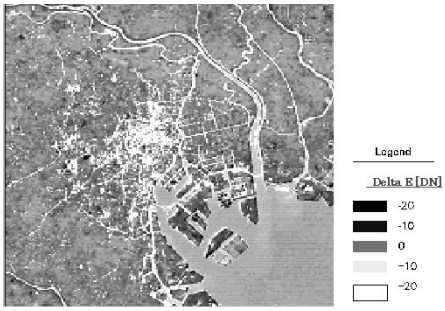

Fig. 6. ΔE image of the central Tokyo.

negative value indicates low thermal infrared radiance. ± 0 indicates an average area of thermal radiance. ΔE is affected by the abnormal thermal radiation in each category but also by other effects such as atmospheric effects, topographic effects, land cover classification errors, and nonlinearities in mixed-pixel radiances. Furthermore, ΔE depends on the image data itself and may not be an inherent land surface parameter. In addition, if multitemporal data are to be analyzed using ΔE, then atmospheric correction is necessary to compensate for seasonal atmospheric variations, and emissivity is also required to be considered because emissivity for each land cover such as vegetation and urban areas can be different.

Fig. 5 shows a ΔE image calculated from results of Fig. 2 and Fig. 4 using (6) at a spatial resolution of 120 m. The spatial resolution of the ΔE image is also 120 m. In Fig. 5, the thermal infrared radiance varies in vegetation areas. The cause of this variation cannot be clarified without a field survey but may be attributable to the difference in thermal radiation from the transpiration of leaves [12]. In addition, Fig. 6 shows an image of Tokyo enlarged from Fig. 5. From Figs. 5 and 6, it can be seen that the thermal infrared radiance value of central Tokyo, especially the downtown area, is greater than those in other cities, and the ΔE value corresponds to major business areas or major roads. The rivers have also a higher ΔE value in central Tokyo. The cause of these variations cannot be clarified without a field survey but may indicate that central Tokyo is discharging more heat than other urban areas. The derivation of ΔE is simple and easy. Moreover, ΔE will give effective information for thermal infrared analysis of remotely sensed imagery.

IV. CONCLUSION

A technique was developed for estimating the thermal infrared radiance of each land cover in a low spatial resolution image using visible and NIR images of higher spatial resolutions. Also, a technique was developed for mapping the thermal infrared radiation variation based on the fact that the temperature is not equal throughout the same category. In the future, these techniques can be applied to the diagnosis of vegetation and evaluation of thermal environments inside cities by analyzing the ΔE in images from season to season.

REFERENCES

[1] R. A. Arnone, "Satellite-derived color-temperature relationship in the Alboran sea," *Remote Sens. Environm.*, vol. 23, pp. 417–437, 1987.

[2] H. U. Solanki, R. M. Dwivedi, and S. R. Nayak, "Synergistic analysis of SeaWiFS chlorophyll concentration and NOAA-AVHRR SST features for exploring marine living resources," *Int. J. Remote Sens.*, vol. 22, pp. 3877–3882, 2001.

[3] J. B. Adams, M. O. Smith, and P. E. Johnston, "Spectral mixture modeling: A new analysis of rock and soil types at the Viking Lander 1 site," *J. Geophys. Res.*, vol. 91, pp. 8098–8112, 1986.

[4] M. Inamura, "Analysis of remotely sensed image data by means of category decomposition," *Electron. Commun. Jpn.*, pt. 2, vol. 71, pp. 241–250, 1988.

[5] M. O. Smith, S. L. Ustin, J. B. Adams, and A. R. Gillespie, "Vegetation in deserts: I. A regional measure of abundance from multispectral images," *Remote Sens. Environ.*, vol. 31, pp. 1–26, 1990.

[6] J. J. Settle and N. A. Drake, "Linear mixing and the estimation of ground cover proportions," *Int. J. Remote Sens.*, vol. 14, pp. 1159–1177, 1993.

[7] J. Settle and N. Campbell, "On the errors of two estimators of sub-pixel fractional cover when mixing is linear," *IEEE Trans. Geosci. Remote Sens.*, vol. 36, pp. 163–170, Jan. 1998.

[8] M. Inamura, H. Toyota, and S. Fujimura, "Apparent temperature patterns superposed on remotely sensed thermal infrared images and their removal" (in Japanese), *J. IEICE*, vol. J 68-D, pp. 981–987, 1985.

[9] M. Inamura, "Improvement of spatial resolution for low spatial resolution thermal infrared image using high spatial resolution visible and near-infrared images" (in Japanese), *J. IEICE*, vol. J 71-A, pp. 497–504, 1988.

[10] M. del Carmen Valdes and M. Inamura, "Spatial resolution improvement of a low spatial resolution thermal infrared image by backpropagated neural networks," *IEICE Trans. Inform. Syst.*, vol. E81-D, pp. 872–880, 1998.

[11] ——, "Spatial resolution improvement of remotely sensed images by a fully interconnected neural network approach," *IEEE Trans. Geosci. Remote Sensing*, vol. 38, pp. 2426–2430, Sept. 2000.

[12] K. Omasa, H. Saji, S. Youssefian, and N. Kondo, *Air Pollution and Plant Biotechnology—Prospects for Phytomonitoring and Phyto-Remediation*. Berlin, Germany: Springer-Verlag, 2002.

[13] K. Oki, H. Oguma, and M. Sugita, "Subpixel classification of alder trees using multitemporal landsat thematic mapper imagery," *Photogramm. Eng. Remote Sens.*, vol. 68, pp. 77–82, 2002.